Supporting Information for:

Resolving Current-dependent Regimes of Electroplating Mechanisms for Fast-Charging Lithium Metal Anodes

David T. Boyle[1,6], Yuzhang Li[2,3,6], Allen Pei[2], Rafael A. Vilá[2], Zewen Zhang[2], Philaphon Sayavong[1], Mun Sek Kim[2], William Huang[2], Hongxia Wang[2], Yunzhi Liu[2], Rong Xu[2], Robert Sinclair[2], Jian Qin[4], Zhenan Bao[4*], & Yi Cui[2,5*]

[1]Department of Chemistry, Stanford University

[2]Department of Materials Science and Engineering, Stanford University

[3]Department of Chemical and Biomolecular Engineering, University of California, Los Angeles

[4]Department of Chemical Engineering, Stanford University

[5]Stanford Institute for Materials and Energy Sciences, SLAC National Accelerator Laboratory

[6]These authors contributed equally.

*Corresponding Authors: yicui@stanford.edu, zbao@stanford.edu

Table of Contents

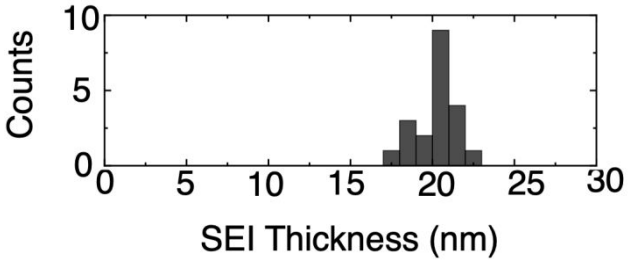

Figure S1. Histogram of SEI thicknesses measured on Li plated in $LiPF_6$ EC:DEC electrolyte using the vitrification and cryo-TEM methods outlined previously.[1] The values show the thickness is about 20 nm. Data adapted with permission from reference ([1]). Copyright 2022 The American Association for the Advancement of Science.

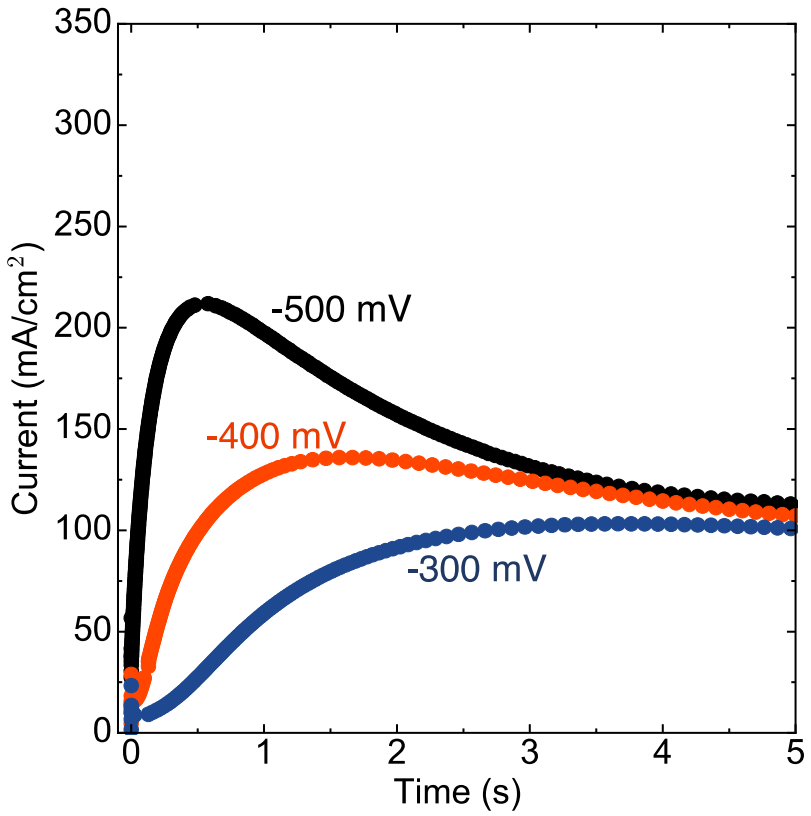

Figure S2. Representative *J-t* profiles for a -500, -400, and -300 mV large *E*-step experiment of Li deposition. The convergence of the current to a similar value at 5 s suggests side reactions and reduction of the electrolyte is not a major contribution to the current.

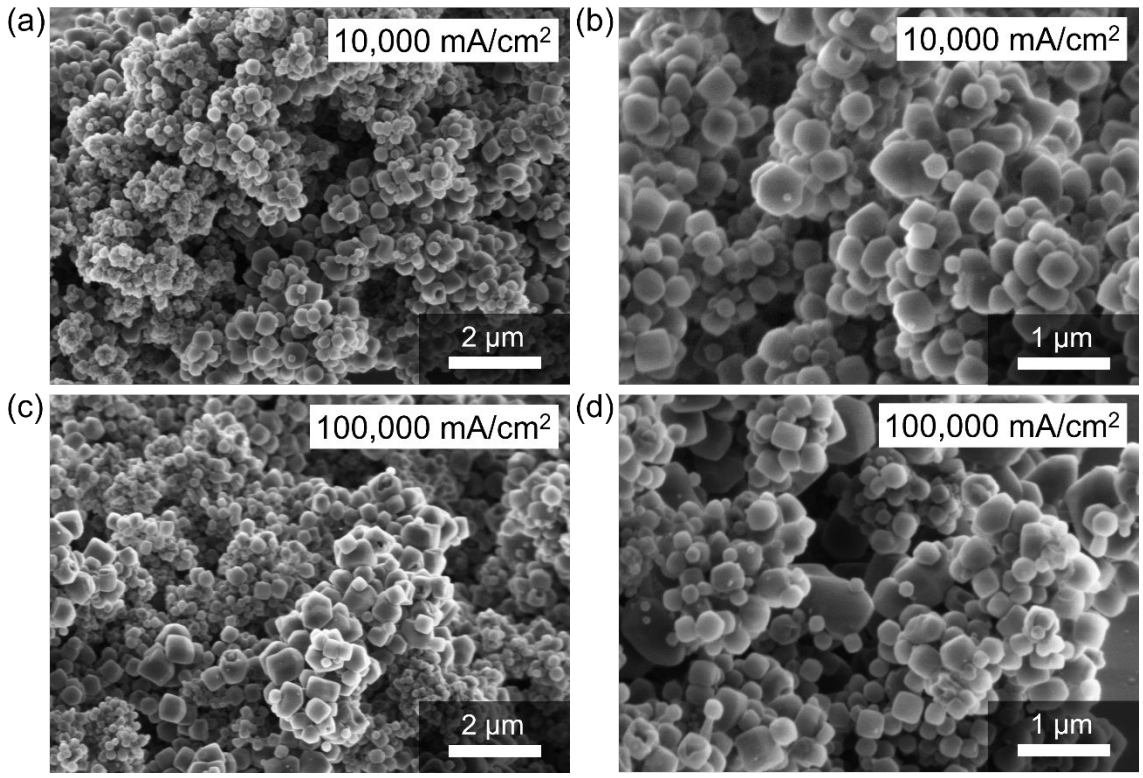

Figure S3. SEM images show that Li electrodeposits as the faceted rhombic dodecahedron morphology when deposited in 1M $LiPF_6$ in EC:DEC at (a,b) 10,000 mA cm^{-2} and (c,d) 100,000 mA cm^{-2} on a tungsten ultramicroelectrode for 0.5 mAh/cm^2.

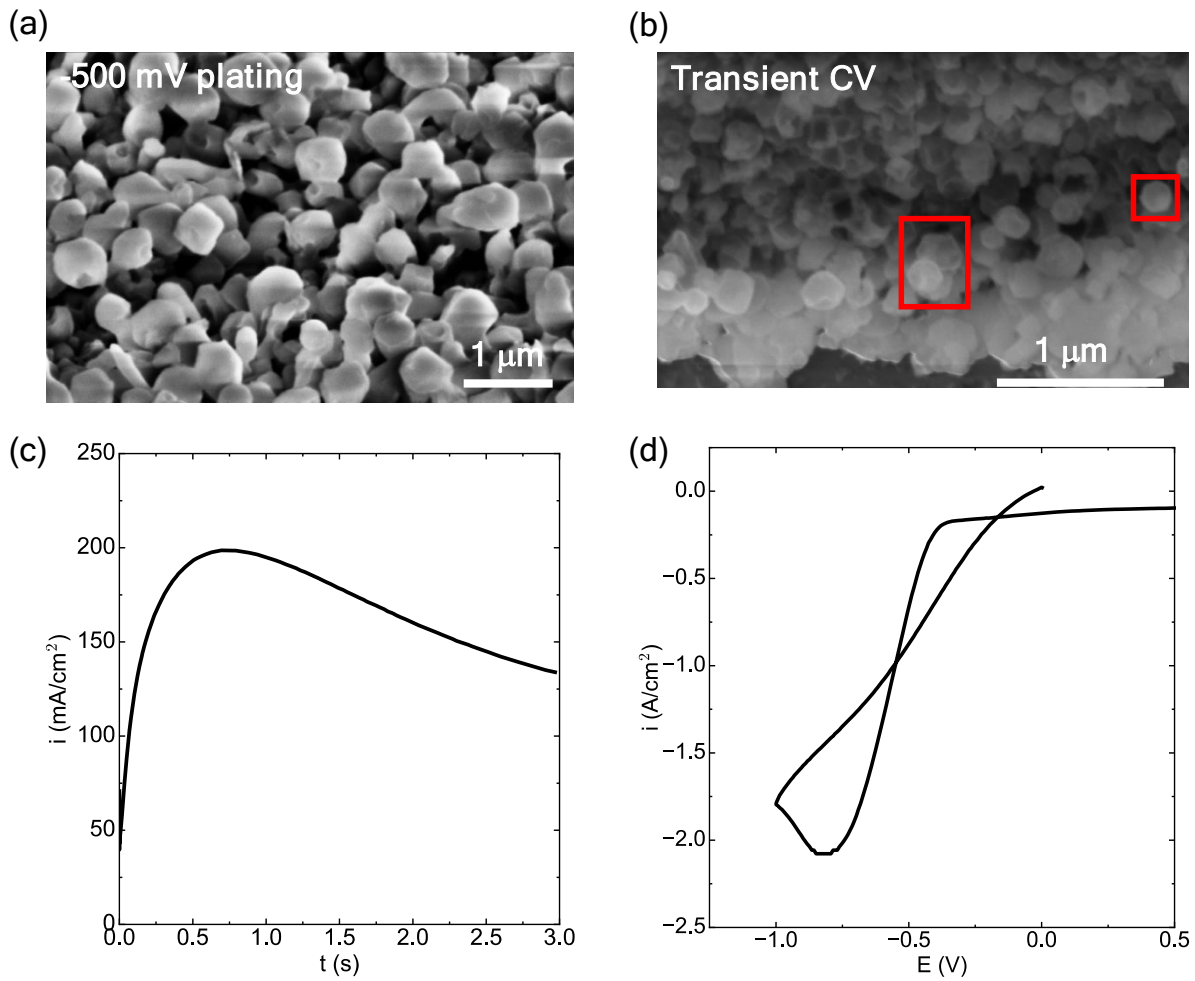

Figure S4. SEM images of electrodeposited Li metal show that faceted particles also form with a large -500 mV *E*-steps (a) and transient CV (b) methods. Immediately after completion of each electrodeposition experiment, the samples were removed from the electrolyte and taken to the SEM. (c) and (d) show the corresponding electrochemical curves used to electrodeposit Li for SEM imaging. Red boxes highlight clearly faceted particles.

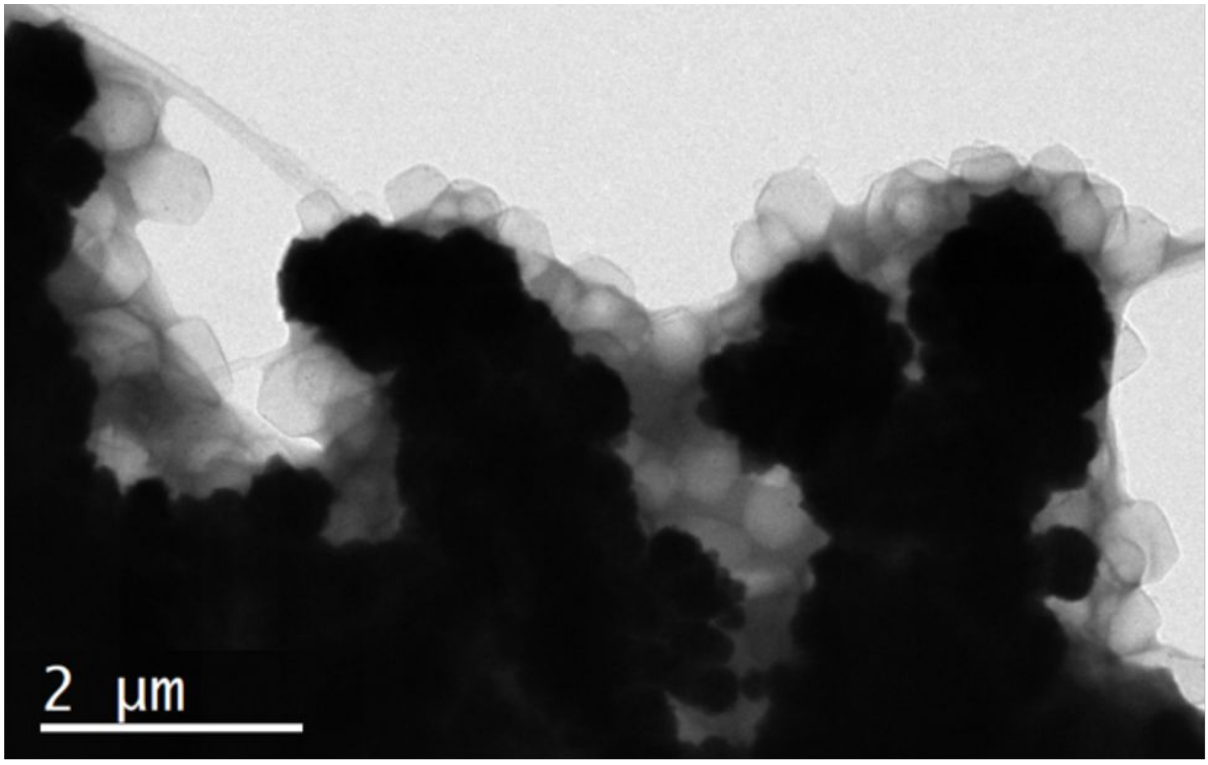

Figure S5. Cryo-TEM image of electrodeposited Li metal on the Cu TEM grid at 100 mA/cm^2. Similar to the images in Figure 3A,B, Li electrodeposits as sharply faceted rhombic dodecahedra at current densities exceeding 100 mA/cm^2, as seen by the edges of sample where Li is electrodeposited. The dark regions of the image correspond to the Cu TEM grid and the lighter contrast particles correspond to Li metal.

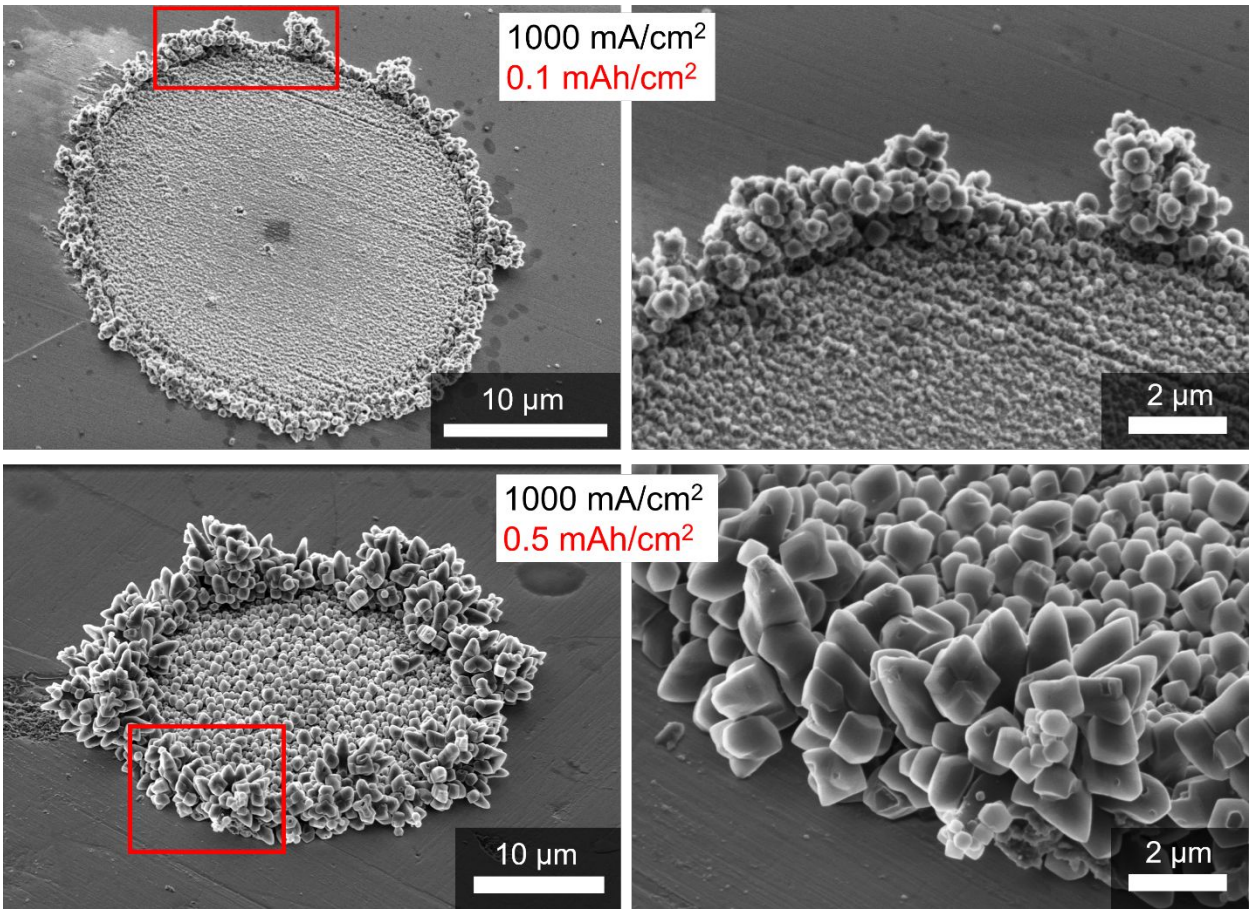

Figure S6. The SEM images show the evolution of the morphology of Li plated at 1,000 mA/cm^2 as a function of capacity on the tungsten ultramicroelectrode. The right panel of images correspond to zoomed-in versions of the portion of the images in the left panels contained in the red box. The increasing width of the individual Li particles from 0.1 to 0.5 mAh/cm^2 suggests that the rhombic dodecahedra grow with tip growth. If the particles were growing from the base, then more columnar filaments with the same radii or width would be expected (see Figure 2d for example), as is commonly observed at low rates in $LiPF_6$ EC:DEC.[2]

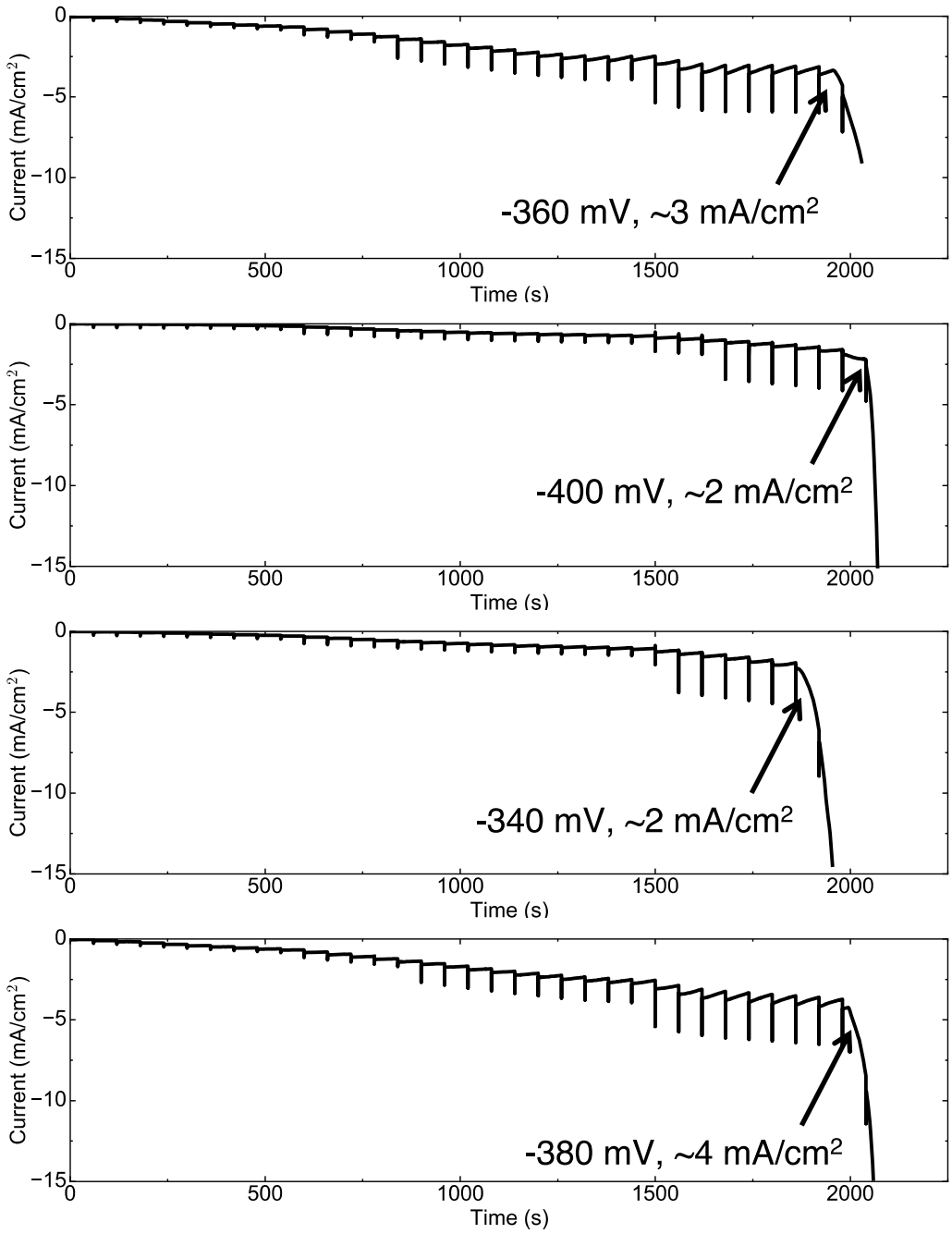

Figure S7. Additional representative experiments demonstrating the reproducibility of the staircase voltammetry measurement exhibiting SEI breakdown. Each panel represents an independent measurement following the same procedure for the data shown in Figure 4A. Hence, the breakdown occurs between a range of -300 to -400 mV and 2-4 mA/cm^2.

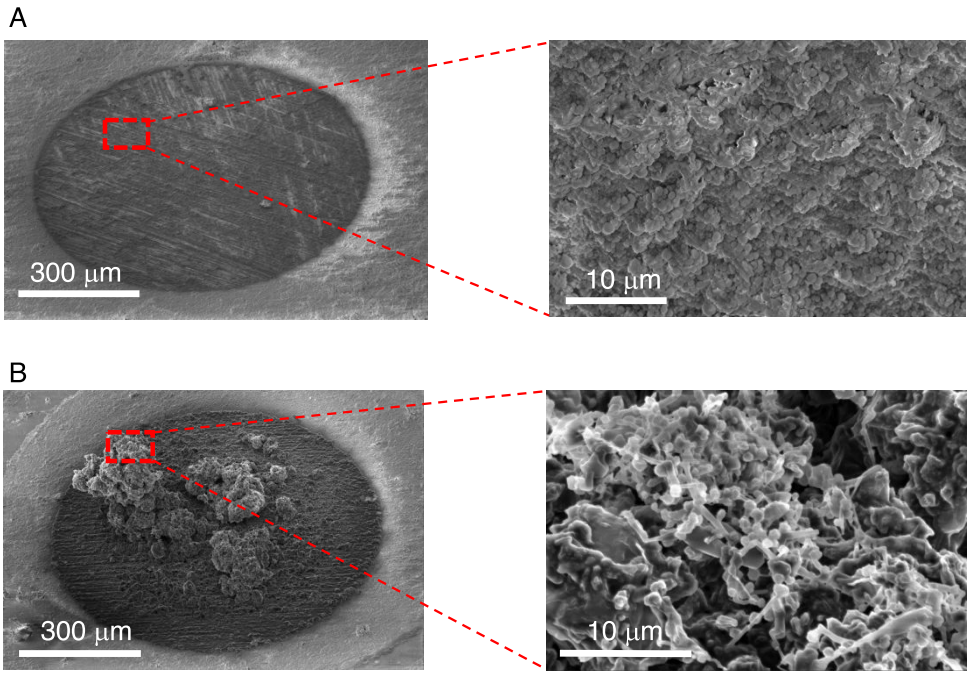

Figure S8. Zoomed in SEM images of electrodeposited Li metal from before and after SEI breakdown during the in the critical potential measurements like that in Figure 4A. (a) Zoomed in SEM image of the Li morphology shown in Figure 4b (I) shows the morphology of Li electrodeposited at low rates in the staircase voltammetry measurement in Figure 4a; the relatively uniform morphology is caused by the reduction of HF in the electrolyte to form the initial SEI on Cu as evident in Figure S9a. (b) Zoomed in SEM image of the Li morphology shown in Figure 4b (III) shows the morphology of Li after SEI breakdown in region (III) of the staircase voltammetry measurement in Figure 4a.

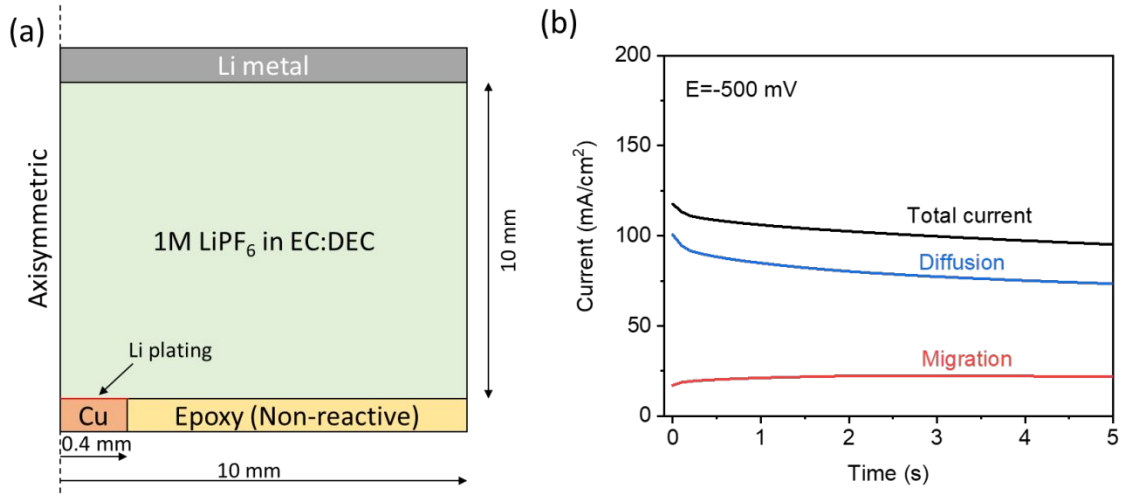

Figure S9. COMSOL simulations for the E-step Li plating. (a) Numerical model for the three-electrode cell, including Cu working electrode, Li counter electrode and Li Reference electrode (not explicitly shown here) (b) Simulated *J-t* profile for a -500 mV *E*-step experiment of Li deposition. The red and blue curves represent the current contributions from Li migration and diffusion, respectively.

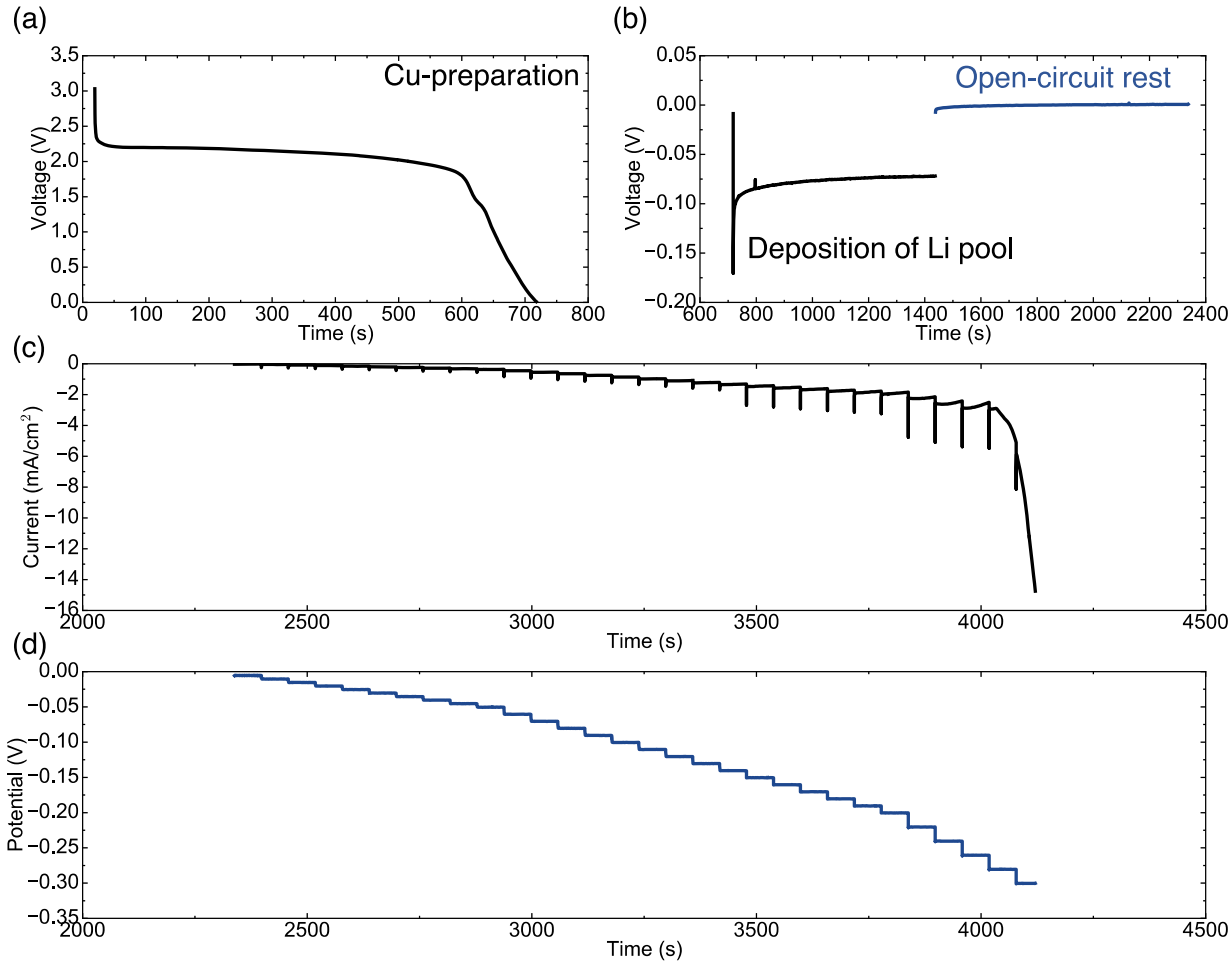

Figure S10. Representative full-set of data for the SEI-breakdown staircase voltammetry measurements in Figure 4. (a) *E*-profile of CuO reduction and SEI formation on the Cu electrode prior to electrodepositing a pool of Li onto the Cu. (b) E-profile highlighting electrodeposition of a 0.1 mAh/cm^2 of Li onto the Cu electrode and the subsequent 15 minute rest at open circuit to form a stable SEI. (c) Measured current vs time as measured for a series of voltage steps (d) from OCV to about -300 mV. The data in (c) are equivalent to Figure 4A.

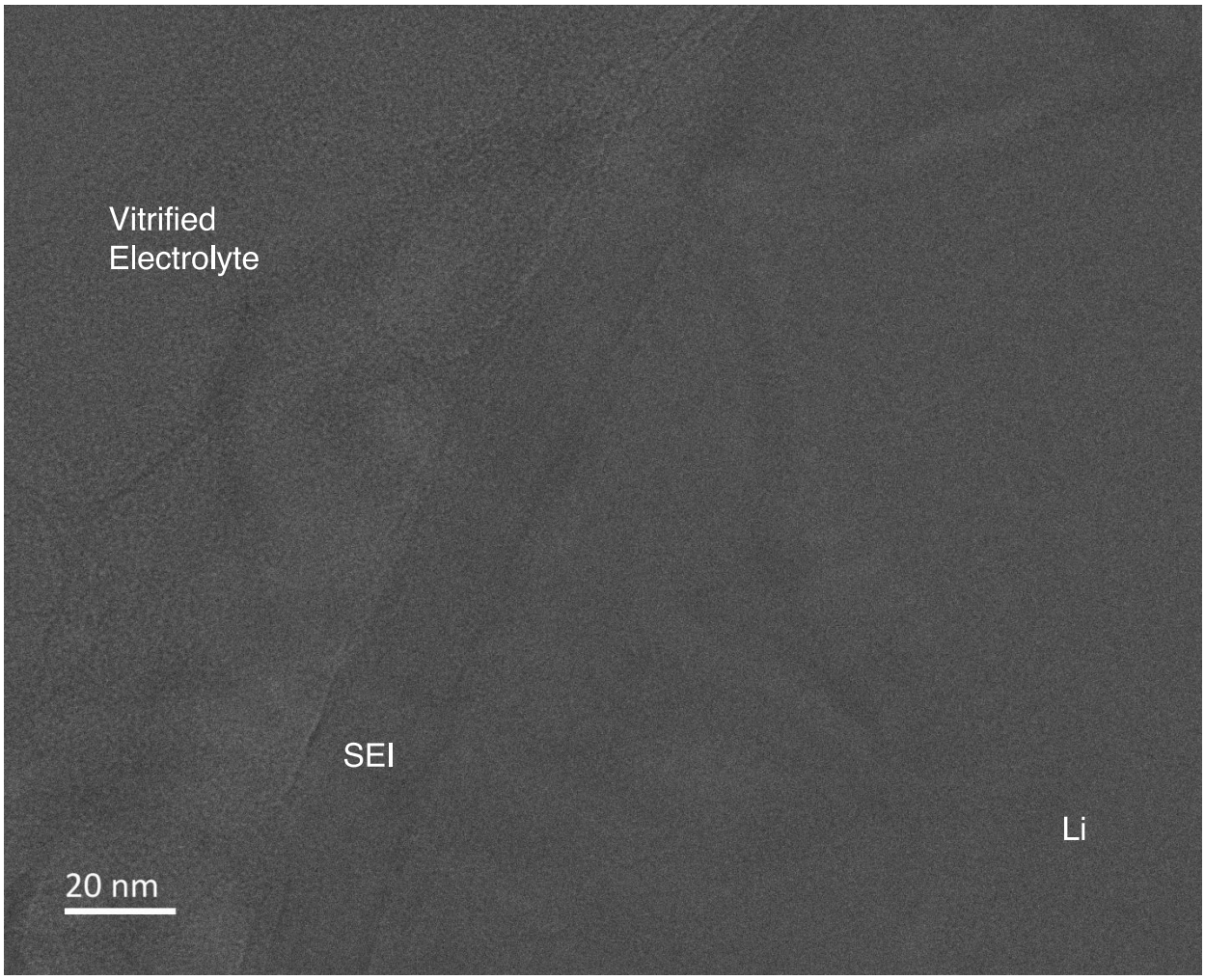

Figure S11. Larger-scale cryo-high resolution TEM image of Li vitrified in the $LiPF_6$ in EC:DEC electrolyte shows the presence of an SEI on Li. The darker band surrounding Li corresponds to the SEI and is caused by the larger density of the SEI compared to Li.

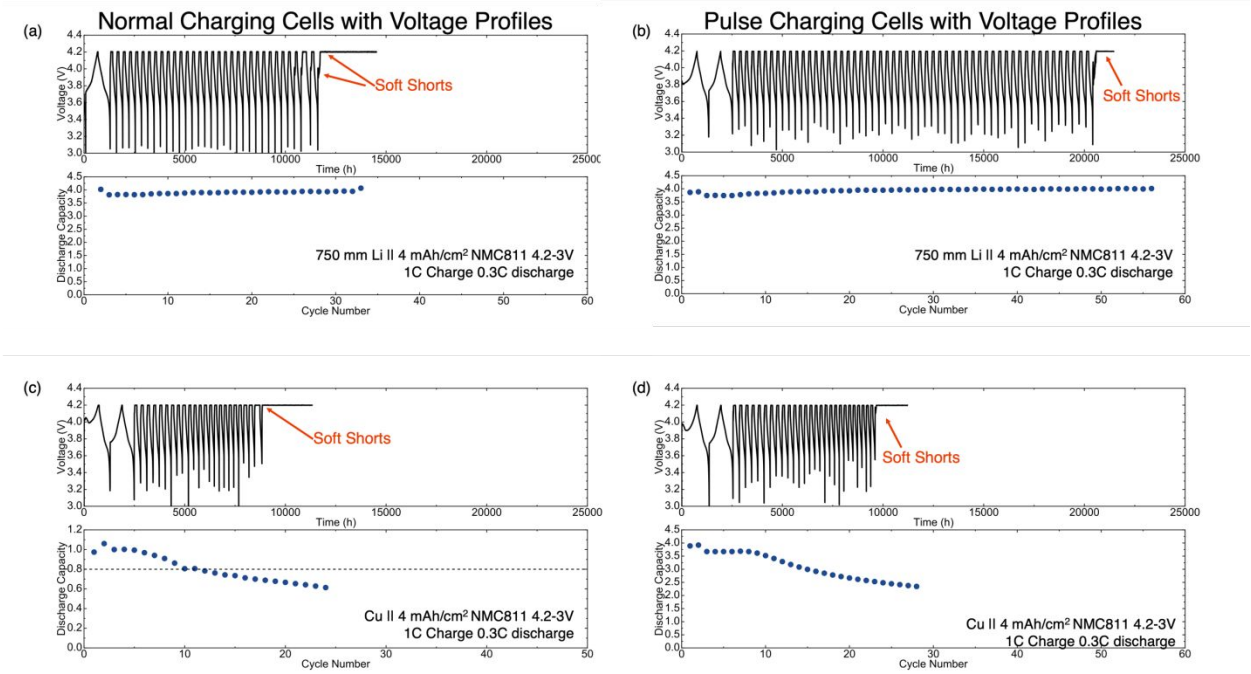

Figure S12. Representative voltage profiles highlighting soft-short failure of the Li||NMC811 full-cells. (a)Voltage profile and corresponding discharge capacity curve from data in Figure 4e for standard cycling with the thick Li foil. The noisy voltage profile and extended hold of during the CV stage of the cycling provide evidence of soft shorting. (b), (c), (d) Voltage profile and corresponding discharge capacity curves from data in Figures 4e,f for pulse charging with thick Li (b), standard charging in anode-free configuration (c), and pulse charging in anode-free (d).

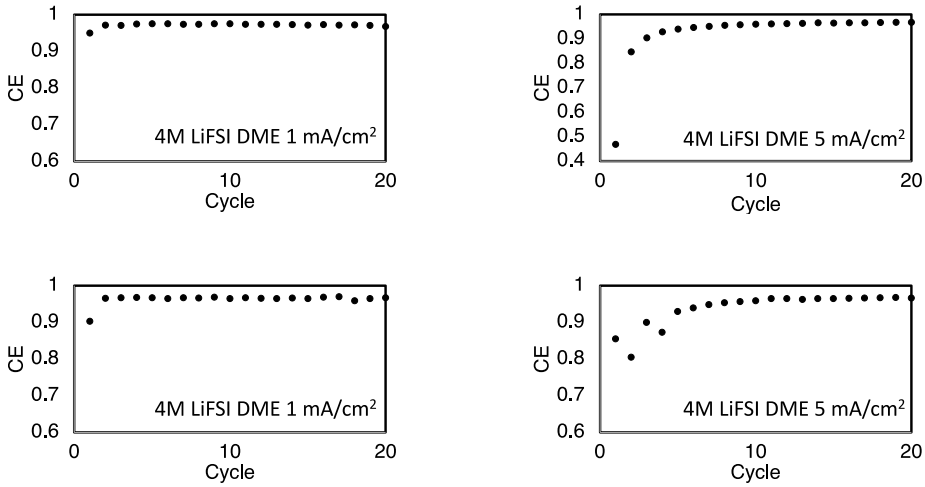

Figure S13. Replicates of CE data for 4M LiFSI in DME from Figure 4b.

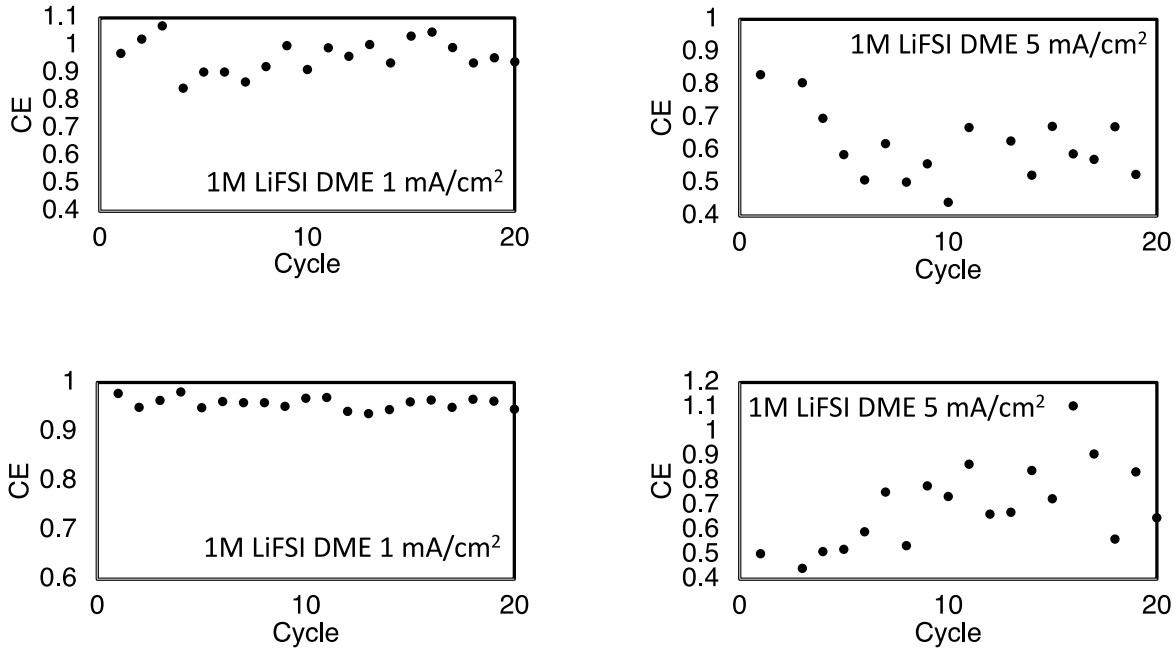

Figure S14. Replicates of CE data for 1M LiFSI in DME from Figure 4a.

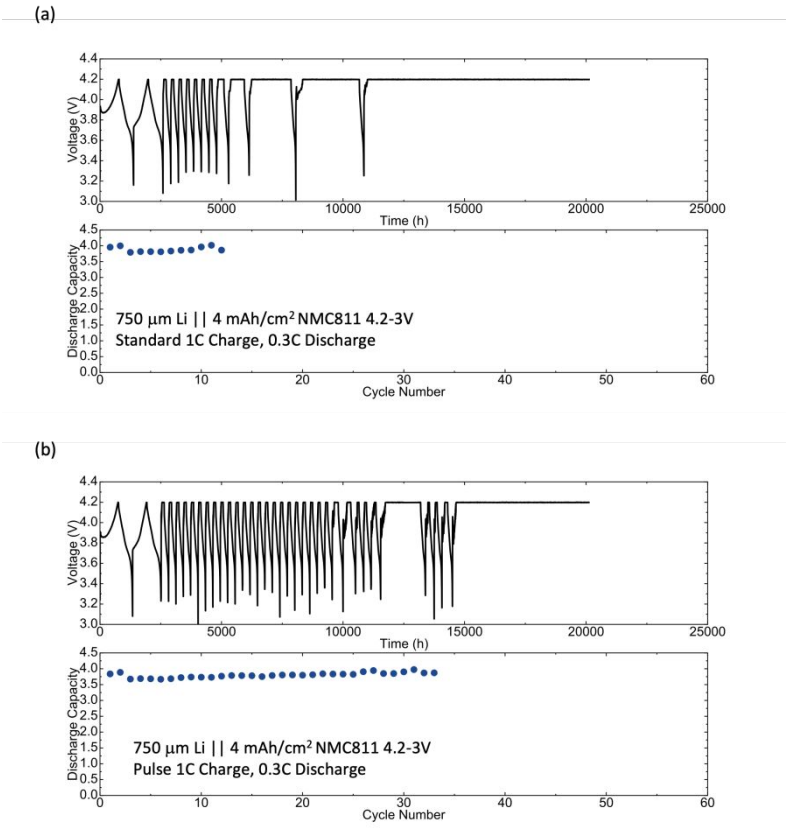

Figure S15. Replicates of full-cell cycling using standard and pulse charging.
(a) Replicate of full cell charging using thick Li foils/large excess of Li with standard 1C charge and 0.3C discharge cycling. The cell can short circuit after using only several cycles using the standard protocol.
(b) Replicate of full cell charging using thick Li foils/large excess of Li with pulse charge and 0.3C discharge cycling**.**

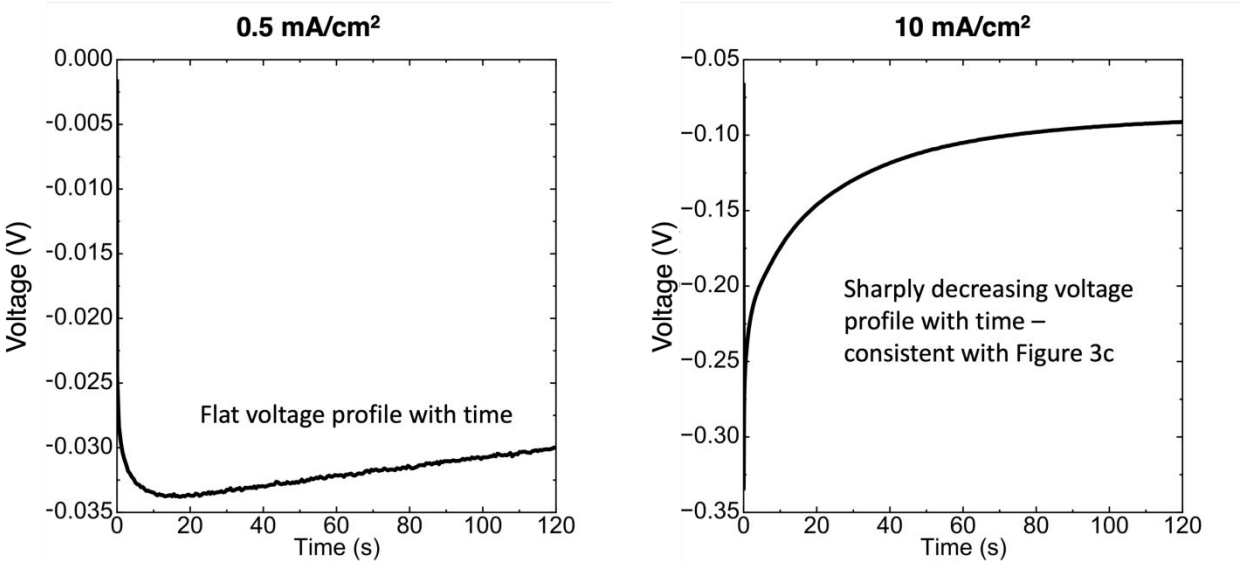

Figure S16. Voltage profiles of direct current steps to currents above and below $J_{\text{crit.}}^{\text{SEI}}$.
(a) Voltage profile of Li plating on Li in the three electrode beaker cell at a low current of 0.5 mA/cm^2. The flat profile suggests there is no SEI breakdown, similar to the staircase measurement. (b) Voltage profile of Li plating on Li in the three electrode beaker cell at a high current of 10 mA/cm^2. The sharp decrease in potential indicates SEI breakdown. This feature is not due to nucleation of Li on Cu, as the plating is occurring on Li. Overall, this figure decouples the effects of capacity and current on SEI breakdown and suggests current is the primary factor.

Table S1. Calculated diffusion coefficients for the large *E*-step methods in cm²/s.

Potential	-500 mV	-400 mV	-300 mV
Trial 1	1.9×10^{-5}	2.1×10^{-5}	5.2×10^{-6}
Trial 2	1.8×10^{-5}	2.6×10^{-5}	5.2×10^{-6}

Tables S1 lists the calculated diffusion coefficients or Li^+ in the electrolyte using the large *E*-step nucleation and growth measurement highlighted in Figure 1i. We note that the values are consistent with the order of magnitude expected for carbonate electrolytes[3], but they deviate slightly from the value calculated with transient LSV (Figure 1h). Deviations of the measured D_{Li^+} between transient LSV and large *E*-step methods likely arise from the sensitivity of the calculation to *A*, the active Li surface area. Transient LSV is the more reliable method, as calculation of D_{Li^+} is independent of *A* (assuming *A* is constant for each υ, which appears true because $\upsilon^{1/2}$ vs. J_p is linear). However, each calculation of D_{Li^+} from the *E*-step method is sensitive to A^2 via $i = \frac{FAC^*_{\mathrm{Li}^+} D^{1/2}_{\mathrm{Li}^+}}{\pi t^{1/2}}$, where *F* is the Faraday constant, so small increases in the true *A* can cause overestimates of D_{Li^+}.[4] Nonetheless, the key conclusion is that the effective D_{Li^+} is much larger than $D^{\mathrm{SEI}}_{\mathrm{Li}^+}$ and closely resemble expected values for bulk electrolytes.

Table S2. Parameters for the EIS measurements and equivalent circuit fits used to calculate Li-ion transport properties of the SEI.

	SEI Thickness (cm)	A (cm^2)	R_s (Ω)	C_{SEI} (F)	R_{SEI} (Ω)	C_{SC} (F)	W ($\Omega \bullet s^{-0.5}$)	λ_{SEI} ($(\Omega cm)^{-1}$)	n_0 (mol/cm^3)	$D_{Li\text{-}ion}$ (cm^2/s)
1	2.0×10^{-6}	2	2.862	1.23×10^{-6}	253.9	4.19×10^{-6}	3637	1.58×10^{-8}	2.54×10^{-6}	1.66×10^{-9}
2	2.0×10^{-6}	2	5.114	5.92×10^{-7}	241.1	4.33×10^{-6}	3714	1.6674×10^{-8}	2.31×10^{-6}	1.92×10^{-9}
3	2.0×10^{-6}	2	3.009	3.03×10^{-7}	265.2	3.20×10^{-6}	4352	1.5158×10^{-8}	1.85×10^{-6}	2.18×10^{-9}
4	2.0×10^{-6}	2	3.441	5.83×10^{-7}	281.8	3.55×10^{-6}	4176	1.4265×10^{-8}	2.14×10^{-6}	1.77×10^{-9}
5	2.0×10^{-6}	2	8.027	7.67×10^{-7}	215.4	3.17×10^{-6}	4535	1.8663×10^{-8}	1.39×10^{-6}	3.58×10^{-9}

Methods

Preparation of Electrolytes

The 1M $LiPF_6$ in EC:DEC electrolyte was used as received from Gotion. This electrolyte was used in most of the paper as the model system because of its extensive characterization in the literature. LiFSI (Oakwood) was dried for 24 hours prior to dissolving into DME (Sigma, anhydrous, 99.5%) and/or TTE (Synquest, 99%). 1 or 4 M LiFSI in DME (mol LiFSI/volume of DME) and 1:1.2:3 molar ratio of LiFSI:DME:TTE were prepared in an argon glovebox. All the electrolytes were handled and stored in an argon-filled glovebox (Vigor, oxygen <1 ppm, water <0.1 ppm) at room temperature.

Electrochemical Impedance Spectroscopy

Symmetric Li||Li 2032-type coin cells were used to measure the interfacial impedance of the SEI in each electrolyte. The cells were prepared in an Argon glovebox with both O_2 and H_2O level below 0.2 ppm. Each cell used two polished and flattened 1cm^2 discs of Li, 60 μL of electrolyte, and a 25-micron thick polypropylene-polyethylene-polypropylene separator (Celgard). A 16-channel electrochemical workstation (VMP3, Biologic Science Instruments) was used for all electrochemical methods unless specified otherwise. The measurements were made at open circuit immediately after assembly (about 5 minutes after contact with electrolyte), and a frequency range of 1 MHz to 0.2 Hz was used with a perturbation amplitude of 5 mV. Each spectrum showed the characteristic depressed semi-circle associated with the impedance of Li metal in nonaqueous electrolytes.[5]

Prior to fitting the data, the raw EIS spectra was averaged between the two equivalent Li electrodes (*i.e.* dividing by two) and normalized to the surface area of one Li electrode (1 cm^2). The impedance data was fit to an equivalent circuit commonly used to describe SEI using ZFit EIS fitting from EC-Lab. The equivalent circuit consists of a capacitor representing the space charge capacitance (C_{SC}), a resistor representing the resistance to Li^+ transport through the SEI (R_{SEI}), and a capacitor representing the dielectric response of the SEI in parallel (C_{SEI}). A Warburg diffusion element representing Li^+ diffusion through the SEI is also included in series with the space charge capacitance. Notably, this equivalent circuit neglects any contribution of interfacial charge transfer resistance (i.e. $Li^+ + e^- \rightarrow Li^0$), but previous measurements of the interfacial electron transfer kinetics suggest this is a reasonable approximation.[6] Several equivalent circuits for SEI give similar results, but the simplicity (only 4 parameters) and accuracy in predicting known features of a model Li_2O SEI of this particular model makes it the most suitable for extracting physical parameters.[7] Only data with a frequency greater than 20 Hz was included for the fit to ensure that the impedance response is related to the compact SEI layer, as opposed to loosely connected clumps of extended SEI.[7,8]

The Nernst-Einstein framework of ionic conductivity was used to calculate the ionic transport parameters of the SEI, similar to previous work with a model Li_2O SEI.[7] The conductivity of the SEI is calculated via $\lambda_{SEI} = \frac{l_{SEI}}{R_{SEI}A}$, where l_{SEI} is the measured thickness of the SEI from cryo-TEM. With λ_{SEI} and the Warburg element (Z_W) from the equivalent circuit fit, $D_{Li^+}^{SEI}$ is then calculable from $Z_W = \frac{D_{Li-ion}^{1/2}}{\lambda_{SEI}A}$. The n_0 of Li^+ in the SEI can then be calculated with the Nernst-Einstein equation $D_{Li^+}^{SEI} = \frac{\lambda_{SEI}RT}{F^2 n_0}$, where R is the standard gas constant and T is the temperature (298 K). A set of parameters for the EIS measurement and calculated parameters for five samples is included in Table S2.

Transient LSV, CV, and Fast Plating of Li on the UME

Homemade UMEs were made by embedding a 25 micron diameter tungsten wire within borosilicate glass. The wire is thread through the glass, and the glass is carefully melted to the wire with a propane blowtorch. The melting process prevented the formation of bubbles between the wire and glass insulation. Once the tungsten wire is sealed in the glass, it is electrically connected to Cu wire with Ag

paste, and the open space of the electrode is filled with insulating polymer. The disc electrodes were polished prior to each experiment with a 0.3 micron and 0.1 micron diamond lapping disc. Each electrode was then rinsed with deionized water and acetone, after which they were quickly dried and transferred to the glovebox transfer chamber. For the UME measurements, iR_u correction was used in all cases except for the galvanostatic plating of Li for SEM imaging. Note that a three-electrode configuration is suitable but unnecessary for the UME measurements, because the nominal current density is so low (~nA range).

For transient LSV and CV measurements, the experiments are run in an argon-filled glovebox, and the UME is swept from OCV in a beaker cell to about -1.2 V vs Li/Li^+ at rates of 10 V/s to 40 V/s and back to 0 V vs. Li/Li^+ for CV. The scan rates were chosen to be consistent with our previous report and are within the range of kinetic irreversibility for the Li electrodeposition reaction in $LiPF_6$ EC:DEC.[6] Importantly, the scan rates are also fast enough to treat the diffusion layer linearly, and treatment of the irreversible voltammograms for metal deposition is identical to the case where the redox species are soluble.[4] The error bars in Figure 1h inset for J_p represent at least three independent measurements. Despite the high concentrations of salt, the low transference number of Li^+ in carbonate electrolyte suggests migration is not a major contribution to the current (Figure S9). For SEM images of Li electrodeposited with transient CV, the UME is removed immediately after Li electrodeposition. For galvanostatic electrodeposition of Li on the UME, the specified current (ranging from 10 to 100,000 mA/cm^2) is applied until 0.5 mAh/cm^2 of Li is electrodeposited. For SEM images, the electrode is removed from the electrolyte immediately after Li deposition, rinsed with about 60 mL of DEC, and transferred to the SEM chamber. An Apreo S LoVac SEM was used for secondary electron imaging Li with 5 kV at room temperature.

Staircase Voltammetry and Large *E*-step Measurements

All staircase voltammetry measurements were carried out with three-electrode and iR_u-corrected beaker cells in an argon-filled glovebox. The iR_u correction was made by taking the high frequency real component of the impedance and using positive feedback voltammetry. Homemade 0.005 cm^2 Cu electrodes insulated with a chemically resistant epoxy were used as the working electrode. The Cu electrode was polished with 2000 grit sandpaper before each experiment. A strip of Li metal foil was used for both the reference and counter electrode. All potentials reported in this paper are vs. the equilibrium potential of Li/Li^+. Prior to running the *E* and *J*-step measurements as shown in Figure 3, the Cu electrode was brought from its open circuit voltage (OCV, ~3 V vs. Li/Li^+) to 10 mV with *J* of -50 $\mu A/cm^2$ to reduce residual CuO and form an SEI layer on Cu (Figure S10a). Once the *E* reached 10 mV, 0.1 mAh/cm^2 of Li was electrodeposited on the Cu surface with a *J* of 0.5 mA/cm^2 to deposit a pool of Li for use as the working electrode in the *E* and *J*-step measurements (Figure S10b). Unless specified otherwise, the cell was held for 15 minutes at OCV to relax any concentration gradients and stabilize the SEI (Figure S10b). The aged sample in Figure 3c was held at OCV for 60 minutes. After aging, the *E* or *J*-step measurements were started. For *E*-step measurements as in Figure 1c and Figure 3a, the potential was increased from -5 mV to -50 mV in increments of 5 mV with 60 second holds. For extended experiments (Figure 3a), the *E* was then increased from -50 mV to -200 mV in increments of 10 mV with 60 second holds and then increased from -200 mV to -400 mV or until the break point was reached in increments of 20 mV with 60 second holds. A representative full set of data that corresponds to the experiment in Figure 3a is shown in Figure S10. *J*-step measurements followed a similar procedure. After preparation of the Cu surface, plating of Li, and rest at OCV, *J* was increased in increments of 0.05 mA/cm^2 from -0.05 to -0.5 mA/cm^2 with 60 second holds.

Then J was increased from -0.5 to -2 mA/cm^2 in increments of 0.1 mA/cm^2 with 60 second holds and from -2 mA/cm^2 to 20 mA/cm^2 in increments of 0.5 mA/cm^2 with 60 second holds or until breakdown occurred. The full experiments are plotted in Figure 3, and the insets show the stacked E or J profiles in the low-rate regime to highlight changes in the profiles. For SEM imaging, the electrode is removed from the electrolyte immediately after stopping the deposition at Li near regions labeled (I), (II), and (III) in Figure 3a, rinsed with about 60 µL of DEC, and transferred to the SEM chamber. An Apreo S LoVac SEM was used for secondary electron imaging with 5 kV at room temperature. The Sand's capacity measurement was calculated using

$$C_{\text{sand}} = \pi D_{\text{Li}^+} \frac{(C_{\text{Li}}^* + F)^2}{4Jt_a^2} \quad (2)$$

where t_a is the anion transference number.[9]

The large E-step measurements in Figure 1f used the same three-electrode cell configuration with iR_u correction as the critical current density measurements. After the Cu was treated with a J of -50 µA/cm^2 to reduce residual CuO and form an SEI layer on Cu, the E was stepped to -300, -400, or -500 mV and the current was measured for about 8 s. The data was then fit the Scharifker model of 3D heterogeneous nucleation and growth[10] with non-linear least-squares fitting. The total current is described by $J = P_3 t^{-\frac{1}{2}} \left(1 - \exp\left(-P_1\left[t - \frac{1-\exp(-P_2 t)}{P_2}\right]\right)\right)$. $P_{1,2,3}$ are the parameters used in the non-linear least-squares fitting. $P_1 = (\frac{8\pi c_0}{\rho})^{\frac{1}{2}} N_0 \pi D_{\text{Li}^+}$, $P_2 = A$, and $P_3 = \frac{F D_{\text{Li}^+}^{1/2} c_0}{\pi^{1/2}}$, where c_0 is the concentration of Li$^+$, ρ is the density of Li metal, N_0 is the number of available nucleation sites, and A is the nucleation rate. The curvefit function from Python and the SciPy package were used for the fitting. Similar to the transient LSV and CV, the low transference number of Li$^+$ in carbonate electrolyte suggests migration is not a major contribution to the current (Figure S9). For SEM images, the electrode is removed from the electrolyte immediately after deposition, rinsed with about 60 µL of DEC, and transferred to the SEM chamber under air-free conditions. An Apreo S LoVac SEM was used for secondary electron imaging with 5 kV at room temperature.

Battery Measurements

Cycling measurements were made with an Arbin instrument. Type 2032 coin-cells were used with a Li Counter/Reference electrode and Cu foil (Pred materials) as the working electrode. Prior to cycling the cells were held at 0 V overnight to reduce residual CuO and form an SEI layer on Cu. Then the cells were cycled using a deposition (charging) rate of either 1 or 5 mA/cm^2 as specified in the main text until a capacity of 1 mAh/cm^2 was reached, and stripping (discharge) rate of 1 mA/cm^2 until a voltage cutoff of 1 V is reached. The ratio of charge input during charge to charge output during discharge quantifies the Coulombic Efficiency. Replicate tests are shown in Figures S13 and S14.

Full-cells also used type 2032 coin-cells. In all cases, NMC811 (Targray, 4 mAh/cm^2) was used as received and cut into 1 cm^2 discs prior to cell assembly. Aluminum coated cathode caps (MTI), 3-stainless steel spacers on the anode side, a 25 micron triple layer separator (Celgard, polypropylene-polyethylene-polypropylene), and 40 µL of LiFSI:DME:TTE electrolyte was used. In anode-free cells a Cu (Pred materials, 1.25 cm^2) was used as the anode. Cells with excess Li used 750 µm thick Li foil. Biologic Science Instruments was used for the room temperature cycling measurements as it is most equipped for rapid pulse charging. All cells underwent two formation cycles with 0.1C charge/discharge. Afterwards, a CCCV or modified pulse-CV protocol was used. The standard methods cycled between 3 and 4.2 V with 1C charge

rate and 0.3 discharge rate, with a hold at 4.2 V until the current reached 0.05C during the charging step. The pulse-CV had an equivalent net charging rate, but the current was alternated between 1.5 and 0.05C for 48 and 25 ms, respectively, until the voltage hit 4.2 V. The ratio was chosen to maintain the 1C net charging rate. The times were chosen to minimize the length of continuous time at the fast-charging rate while being in a range that allows for double layer charging and discharging, which is typically on the order of 10s of ms for a 1 cm^2 electrode.[4] The battery was then charged at 1C until hitting 4.2 V again and underwent the voltage hold at 4.2 V to a 0.05C cutoff. The same 0.3C discharge rate was used. Replicate tests are shown in Figure S15. NMC is chosen as the cathode to ensure that excess Li is left on the Cu current collector in anode-free cells, so Li is plating on Li.

Characterization Methods

Measurements of the SEI thickness were as reported in our previous work.[1] Samples were prepared in 2032-type coin-cells with 60 μL of electrolyte with Li metal and a Quantifoil TEM grid coated with roughly 200 nm of evaporated Cu electrode as the electrodes. Li was electrodeposited directly onto the TEM grid. Immediately after deposition, the coin cells were disassembled in an argon-filled glovebox. Residual electrolyte on the TEM grid were removed via a manual double-side blotting method with filter paper and tweezers. Typical blotting procedure takes about 3 to 5 s for one side. The TEM grid was then sealed in an airtight container and immediately submerged and broken in liquid nitrogen to expose the sample to cryogen without air exposure. The sample was then loaded into the Gatan side-entry cryo-transfer holder (Gatan 626) and inserted into the TEM column at liquid N_2 temperatures. This specialized cryo-transfer holder with a shutter prevents air exposure and condensation onto the sample. Inside the TEM column, the sample temperature was maintained at about -173 to -178 ^{0}C during imaging. Imaging was performed with a Thermofisher Titan 80-300 environmental (scanning) transmission electron microscope operated at an accelerating voltage of 300 kV. The instrument is equipped with an aberration corrector in the image-forming lens, which was tuned before each sample analysis. Cryo-TEM images were acquired by a Gatan K3 IS direct-detection camera in the electron-counting mode. One or two short exposure (0.1 s) single-frame shots were taken to estimate the defocus and make it as close as possible to Scherzer defocus. Cryo-EM images were taken with an electron dose rate of around 45 $e^-/Å^2/s$, a total of 5 frames were taken with 0.1 s per frame for each image. To measure the SEI thickness, the intensity across the interfacial layers were summed over around 300-500 pixels along the dendrite direction. The thickness could be extracted by identifying the distance between sharp intensity changes. Values of the SEI thickness were compiled from several independent samples. To improve statistical reliability as much as possible, each data point was taken from an independent Li filament.

Samples for crystallographic analysis of the rhombic dodecahedra were prepared in 2032 type coin-cells with 60 μL of electrolyte. Coin cells were constructed with Li metal as the counter/reference, separator, liquid electrolyte, and Cu TEM grid as the current collector. The Cu TEM grid was prepared by electrodepositing Cu onto a stainless steel TEM grid at -0.88 V vs. the regular hydrogen electrode for a total of 1.1 mAh/cm^2. Li was deposited onto the Cu TEM grid substrate at 100 mA/cm^2 for about 0.2 mAh/cm^2. After deposition, coin cells were disassembled in Ar glovebox and the TEM grid substrate rinsed with ~30 uL of 1,3-dioxolane to remove Li salts. The sample then remained in liquid N_2 throughout the duration of the cryo-transfer process using Gatan 626 holder and transfer station. Cryo-EM samples did not need to be sectioned or thinned; they were imaged as is to preserve their native shape and chemistry. All TEM images shown are taken on Titan E(S)TEM 80-300 kV. The sample temperature was maintained at about -173 to -178 ^{0}C during imaging. Images shown are brightfield TEM images taken at 300 kV

accelerating voltage. To align faceted Li metal particles along the zone axis, the sample was tilted appropriately within a +/- 15 degree angle (some searching was necessary but samples could be found properly aligned within 15-20 minutes).

References

(1) Zhang, Z.; Li, Y.; Zhou, W.; Li, Y.; Oyakhire, S. T. .; Boyle, D. T. .; Wu, Y.; Xu, J.; Wang, H.; Yu, Z.; et al. Capturing the Swelling of Solid-Electrolyte Interphase in Lithium Metal Batteries. *Science* **2022**, *70*, 66–70.

(2) Lin, D.; Liu, Y.; Cui, Y. Reviving the Lithium Metal Anode for High-Energy Batteries. *Nat. Nanotechnol.* **2017**, *12* (3), 194–206.

(3) Hayamizu, K.; Aihara, Y.; Arai, S.; Martinez, C. G. Pulse-Gradient Spin-Echo 1H, 7Li, and 19F NMR Diffusion and Ionic Conductivity Measurements of 14 Organic Electrolytes Containing $LiN(SO_2CF_3)_2$. *J. Phys. Chem. B* **1999**, *103* (3), 519–524.

(4) Bard, A. J.; Faulkner, L. R. *Fundamentals and Applications*; John Wiley and Sons, Inc.: New Jersey, 2001.

(5) Aurbach, D. *Nonaqueous Electrochemistry*; Dekker, M., Ed.; New York, 1999.

(6) Boyle, D. T.; Kong, X.; Pei, A.; Rudnicki, P. E.; Shi, F.; Huang, W.; Bao, Z.; Qin, J.; Cui, Y. Transient Voltammetry with Ultramicroelectrodes Reveals the Electron Transfer Kinetics of Lithium Metal Anodes. *ACS Energy Lett.* **2020**, *5*, 701–709.

(7) Guo, R.; Gallant, B. M. Li_2O Solid Electrolyte Interphase: Probing Transport Properties at the Chemical Potential of Lithium. *Chem. Mater.* **2020**, *32*, 5525–5533.

(8) Boyle, D. T.; Huang, W.; Wang, H.; Li, Y.; Chen, H.; Yu, Z.; Zhang, W.; Bao, Z.; Cui, Y. Corrosion of Lithium Metal Anodes during Calendar Ageing and Its Microscopic Origins. *Nat. Energy* **2021**, *6*, 487–494.

(9) Bai, P.; Li, J.; Brushett, F. R.; Bazant, M. Z. Transition of Lithium Growth Mechanisms in Liquid Electrolytes. *Energy Environ. Sci.* **2016**, *9*, 3221–3229.

(10) Scharifker, B. R.; Mostany, J. Three-Dimensional Nucleation with Diffusion Controlled Growth. Part I. Number Density of Active Sites and Nucleation Rates per Site. *J. Electroanal. Chem.* **1984**, *177* (1–2), 13–23.